

# Triggering and probing of phase-coherent spin packets by time-resolved spin transport across an Fe/GaAs Schottky barrier

L. R. Schreiber,<sup>1,2</sup> C. Schwark,<sup>1,2</sup> S. Richter,<sup>1,2</sup> C. Weier,<sup>1,2</sup> G. Güntherodt,<sup>1,2</sup> C. Adelman,<sup>3</sup> C. J. Palmström,<sup>4</sup> X. Lou,<sup>5</sup> P. A. Crowell,<sup>5</sup> and B. Beschoten<sup>1,2,\*</sup>

<sup>1</sup>*II. Institute of Physics, RWTH Aachen University, 52074 Aachen, Germany*

<sup>2</sup>*JARA: Fundamentals of Future Information Technology, 52074 Aachen, Germany*

<sup>3</sup>*Department of Chemical Engineering and Materials Science, University of Minnesota, Minneapolis, Minnesota 55455*

<sup>4</sup>*Department of Electrical and Computer Engineering and Department of Materials, University of California at Santa Barbara, Santa Barbara, California 93106*

<sup>5</sup>*School of Physics and Astronomy, University of Minnesota, Minneapolis, Minnesota 55455*

(Dated: September 3, 2018)

## Abstract

Time-resolved electrical spin transport is used to generate and probe spin currents in GaAs electrically. We use high bandwidth current pulses to inject phase-coherent spin packets from Fe into  $n$ -GaAs. By means of time-resolved Faraday rotation we demonstrate that spins are injected with a clearly defined phase by the observation of multiple Larmor precession cycles. We furthermore show that spin precession of optically created spin packets in  $n$ -GaAs can be probed electrically by spin-polarized photo-current pulses. The injection and detection experiments are not direct reciprocals of each other. In particular, we find that interfacial spin accumulation generated by the photocurrent pulse plays a critical role in time-resolved electrical spin detection.

Spintronic devices which are based on coherence of an electron spin ensemble require a means to trigger all individual spins with a well-defined phase. Both temporal and spatial phase triggering can easily be achieved by optical orientation using either circularly [1–6] or linearly polarized [7] laser pulses. This triggering results in a macro-phase of the spin ensemble. In a transverse magnetic field all individual spins of this ensemble start to precess from the identical spin orientation, i.e. with the same phase. The coherence of the spin ensemble can be probed by spin precession using time-resolved (TR) magneto-optical techniques [1–7]. In dc spin transport experiments, however, there is only a spatial phase triggering of the spin orientation after electrical spin injection, which is defined by the magnetization direction of the ferromagnetic injector [8–14]. After injection, individual spins start to precess in a transverse magnetic field. This results in a rapid depolarization of the steady-state spin polarization (the Hanle effect), because spins are injected continuously in the time domain. During precession the phase relation is partially preserved when there is a well-defined transit time of a spin between the source and detector [15, 16]. While several spin precessions have been observed in spin transport devices based on silicon [16–18], only very few precessions are seen in drift-based spin transport devices [15, 19, 20]. Despite recent progress in realizing all-electrical spintronic devices, electrical phase triggering and time-resolved electrical readout have not been achieved.

In this Letter we report on TR electrical spin injection (TRESI) and electrical detection of spin currents across an Fe/GaAs Schottky barrier by combining ultrafast electrical and optical techniques. Our device consists of a highly doped Schottky tunnel barrier formed between an epitaxial iron (Fe) and a (100) *n*-GaAs layer. We have chosen this device design for three reasons: (I) the Schottky barrier profile guarantees large spin injection efficiencies [10, 12], (II) the *n*-GaAs layer is Si doped with carrier densities near the metal-insulator transition ( $n = 2 - 4 \times 10^{16} \text{ cm}^{-3}$ ), which provides long spin dephasing times  $T_2^*$  [1, 7, 21] and (III) the Fe injector has a two-fold magnetic in-plane anisotropy [15], which allows for a non-collinear alignment between the external magnetic field direction and the magnetization direction of the Fe layer and thus the polarization direction of the electrically injected spin packets. This non-collinear alignment allows to induce Larmor precession of the spin ensemble.

Our measurement setup for TRESI and the sample geometry are depicted in Fig. 1(a) (see also Ref. [22]). The magnetic easy axis (EA) of the Fe layer is oriented along the GaAs [110]

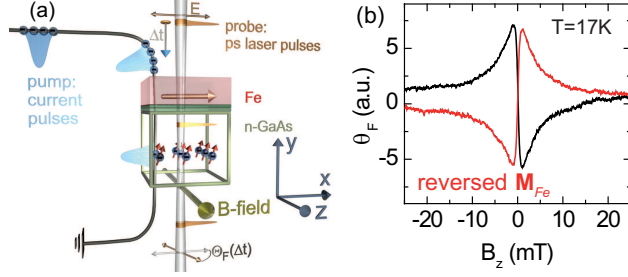


Figure 1: (color online). (a) Schematic of the time-resolved electrical spin injection experiment. (b) Faraday rotation  $\theta_F$  from dc electrical spin injection vs  $B_z$ . Spins are probed in  $n$ -GaAs along  $y$  before (black line) and after (red line) reversing the Fe magnetization  $\mathbf{M}_{Fe}$ .

( $\pm x$  direction)(see Fig. 2(a) in Ref. [22]). The samples are mounted in a magneto-optical cryostat with a magnetic field  $B$  oriented along the  $\pm z$  direction. We apply a current pulse train using high frequency contacts. Linearly polarized ps laser pulses at normal incidence to the sample plane and phase-locked to the electrical pulses monitor the  $\pm y$  component of spins injected in the GaAs by detecting the Faraday rotation angle  $\theta_F$ . The time-delay  $\Delta t$  between the current pump pulses and optical probe pulses is adjusted by an electronic phase shifter.

We first use static measurements of  $\theta_F$  to demonstrate electrical spin injection from Fe into  $n$ -GaAs [Fig. 1(b)]. At reversed bias and  $B_z = 0$  T, injected spins are oriented parallel to the EA of the Fe layer yielding  $\theta_F = 0$ . At small  $B_z$ , spins start to precess towards the  $y$ -direction yielding  $\theta_F \neq 0$ . Changing the sign of  $B_z$  inverts the direction of the spin precession which results in a sign reversal of  $\theta_F$ . As expected [15], the direction of spin precession also inverts when the magnetization  $\mathbf{M}_{Fe}$  is reversed (see red curve in Fig. 1(b)).  $\theta_F$  approaches zero at large  $B_z$ , since the continuously injected spins dephase due to Larmor precession causing Hanle depolarization.

For TRESI, we now apply current pulses with a width of  $\Delta w = 2$  ns and a repetition time of  $T_{rep} = 125$  ns with  $T_{rep} > T_2^*$ . The corresponding TRFR data are shown in Figs. 2(a), 2(b) at various  $B_z$  and  $T = 17$  K. Most strikingly, we observe precession of the injected spin packets at the Larmor frequency  $\omega_L$ , demonstrating that the current pulses trigger spin currents with a well-defined phase. It is apparent that the amplitude of  $\theta_F$  diminishes with increasing  $|B_z|$ , and the oscillations in  $\theta_F$  are not symmetric about the zero base line (see

black lines in Fig. 2a as guides to the eye). For quantitative analysis we use the ansatz

$$\begin{aligned} \theta_F(\Delta t, B_z) = & A(B_z) \exp\left(-\frac{\Delta t}{T_2^*(B_z)}\right) \sin(\omega_L \Delta t + \phi) + \\ & + A_{bg}(B_z) \exp\left(-\frac{\Delta t}{\tau_{bg}}\right), \end{aligned} \quad (1)$$

where the second term accounts for the non-oscillatory time dependent background. The fits to the data are shown in Fig. 2(a) as red curves. We determine a field independent  $\tau_{bg} = 8 \pm 2$  ns and deduce  $|g| = 0.42 \pm 0.02$  from  $\omega_L$ , demonstrating that the spin precession is detected in the *n*-GaAs layer [1]. The extracted spin dephasing times  $T_2^*(B_z)$  and amplitudes  $A(B_z)$  are plotted in Figs. 2(c) and 2(d), respectively. The longest  $T_2^*(B_z)$  values, which exceed 65 ns, are obtained at small  $B_z$ . The observed  $1/B_z$  dependence of  $T_2^*$  (see red line in Fig. 2(c)), which indicates inhomogeneous dephasing of the spin packet, is consistent with results obtained from all-optical TR experiments on bulk samples with similar doping concentration [1]. On the other hand, the strong decrease of  $A(B_z)$  (Fig. 2(d)) has not previously been observed.

The  $A(B_z)$  dependence might be caused by  $B_z$  acting on the direction of the magnetization  $\mathbf{M}_{Fe}$  of the Fe injector. Increasing  $B_z$  rotates  $\mathbf{M}_{Fe}$  away from the easy (*x*-direction) towards the hard axis (*z*-direction). This rotation diminishes the *x*-component of the injected spin packet, which would result in a decrease of  $A(B_z)$ . We calculated this dependence (see dashed line in Fig. 2(d)) for a macro-spin along  $\mathbf{M}_{Fe}$  using in-plane magnetometry data of the Fe layer[22]. The resulting decrease, however, is by far too small to explain our  $A(B_z)$  dependence. To summarize, there are two striking observations in our TRESI experiments: (I) the strong decrease of  $A$  vs  $B_z$  and (II) the non-oscillatory background  $\tau_{bg}$  in  $\theta_F$  independent of  $B_z$ . As both have not been seen in all-optical time-resolved experiments, it is suggestive to link these properties to the dynamics of the electrical spin injection process.

During TRESI, the depletion layer at the Schottky barrier (see band diagram in Fig. 3(a)) acts like a capacitance. When a current pulse is transmitted through the barrier, this capacitance will be charged and subsequently discharged. The charging and discharging can directly be measured by time-domain reflectometry (TDR) (see ref. [22] for details) using a sampling oscilloscope. For TDR we apply a voltage step to the sample with an amplitude of -0.5 V and a rise time of 100 ps at  $T = 20$  K. The time-evolution of the reflected voltage step is shown in the inset of Fig. 3(b). Note that there is a significant temporal broadening

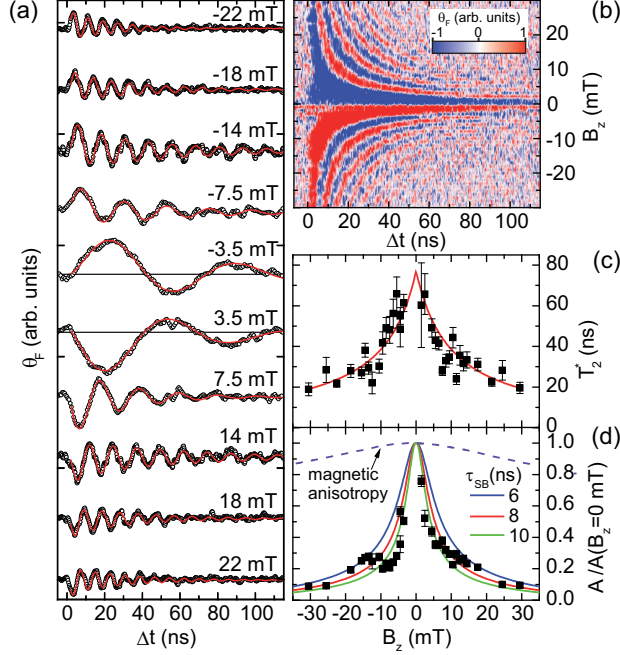


Figure 2: (color online). (a) Faraday rotation  $\theta_F$  vs delay  $\Delta t$  for various magnetic fields  $B_z$  at  $T = 17$  K with vertical offsets for clarity. The red lines are fits to the data. (b) False color plot of  $\theta_F$  vs  $\Delta t$  and  $B_z$ . (c) Spin dephasing time  $T_2^*(B_z)$  and (d) normalized  $\theta_F$  amplitudes  $A$  vs  $B_z$ . The red solid lines in (c) are least-squares fits to the data for  $\Delta t > 2$  ns and solid lines in (d) are simulations for different  $\tau_{SB}$ . The dashed line is the expected decrease of  $A$  due to the rotation of the magnetization of the Fe layer.

of the voltage step with a time constant of 6 ns. We obtain a similar time constant of 6 ns for the discharging process (not shown).

To further link these properties to the pulsed electrical spin injection process, we depict a simple equivalent network of the sample in Fig. 3(a). In the reverse-bias regime, the Schottky contact can be modeled by a Schottky capacitance  $C_s$  and a parallel tunnel-resistance  $R_s$ . The underlying  $n$ -GaAs detection layer is represented by a resistance  $R$  in series. We assume the displacement current  $I_c$  to be unpolarized, while the tunneling current  $I_t$  carries the spin polarized electrons. The spin current  $I_p = \eta I_t$  is given by the spin injection efficiency  $\eta$ . The charging and discharging of the Schottky capacitance is thus directly mapped to the temporal evolution of the spin current.  $I_p$  increases after the current pulse is turned on, whereas it decreases after the pulse is turned off after time  $\Delta w$ , i.e. during the discharge of  $C_s$ . If  $C_s$ ,  $R_s$  and  $\eta$  are approximately bias-independent, the increase and decrease of  $I_p$  is a

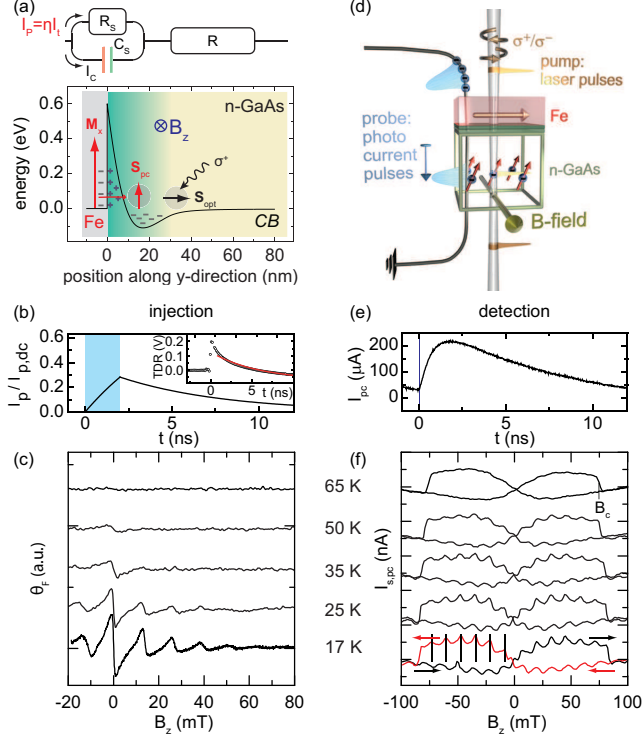


Figure 3: (color online) (a) Simple equivalent network of sample and energy diagram of conduction band. (b) Simulation of the evolution of the spin-polarized tunnel current through the Schottky barrier triggered by a 2 ns long current pulse (light blue). (inset) TDR of voltage step function (-0.5 V) with least-squares exponential fit (red solid line). (c) RSA measurements of  $\theta_F$  vs  $B_z$  at various  $T$  with vertical offsets for clarity. (d) Schematic of optical pump/photo-current probe experiment. (e) Measured photo-voltage pulse. (f) RSA measurements of spin photo-current at various  $T$ .

simple exponential with a time constant  $\tau_{SB} = C_S / (\frac{1}{R} + \frac{1}{R_S})$  as illustrated in Fig. 3(b) for a pulse width of  $\Delta w = 2$  ns and  $\tau_{SB} = 6$  ns.

It is important to emphasize that the electrically injected spin packets are temporally broadened by an amount  $\tau_{SB}$ . This broadening becomes particularly important as individual spins start to precess in  $B_z$  at all times during the spin pulse. The retardation of spin precession results in dephasing of the spin packet and a decrease of the average spin. The temporal evolution of the packet can be estimated by

$$M_y(B_z, \Delta t) = \int_0^{\Delta t} dt r_S(t) M_S(\Delta t - t), \quad (2)$$

where  $r_S(t) = I_p(t)/a$  is the spin injection rate with the active sample area  $a$  and where

$M_S$  is given by an exponentially damped single spin Larmor precession. The integral can be solved analytically [22] and results in a form as given by Eq. 1, motivating our original ansatz. Note that the non-precessing background signal of  $\theta_F$  (see Fig. 2(a)) stems from the discharging of the Schottky capacitance, i.e.  $\tau_{SB} = \tau_{bg}$ , while  $T_2^*$  is not affected by the integration. The amplitude  $A(B_z)$  in Eq. 1 becomes a function of  $\omega_L, T_2^*, \tau_{SB}, \Delta w$  and  $r_s$  (see Eqs. 12/15 in Ref. [22]). For simulating  $A(B_z)$ , we take the results from Fig. 2, i.e.  $T_2^*(B_z), \omega_L$ , as well as  $\Delta w = 2$  ns and vary only  $\tau_{SB}$  as a free parameter. The resulting  $A(B_z)$  curves are plotted in Fig. 2(d) for various  $\tau_{SB}$ . The experimental data are remarkably well reproduced for the  $\tau_{SB}$  values determined by TDR ( $\tau_{SB} = 6$  ns) and by the non-oscillatory background of  $\theta_F$  ( $\tau_{SB} = 8$  ns). This demonstrates that charging and discharging of the Schottky capacitance is the main source of the amplitude drop in our experiment, which limits the observable precession amplitude.

We next explore how this phase coherence, i.e. spin precession, can be probed by electrical means. Here, we use circularly ( $\sigma^+/\sigma^-$ ) polarized ps laser pump pulses with laser energy above the GaAs band edge ( $E = 1.54$  eV) to optically excite coherent spin packets  $\mathbf{S}_{opt}$  in the  $n$ -GaAs layer (Fig. 3(d)) near the degenerate region which is formed close to the Fe/GaAs interface (Fig. 3(a)). The spins generated directly by this pulse, denoted  $\mathbf{S}_{opt}$  in Fig. 3(a), flow into the GaAs bulk and are oriented perpendicular to the interface. The optical pulse also generates a photocurrent (PC) which is spin-polarized due to the replacement of electrons in the interfacial region by carriers tunneling from the ferromagnet [23–25]. This spin-polarization, denoted  $\mathbf{S}_{pc}$  in Fig. 3(a), is oriented parallel to the interface. Fig. 3(e) shows the temporal evolution of the PC as measured by a sampling oscilloscope. As expected, the PC pulse is temporally broadened by the Schottky barrier, similar to the injection pulse in TRESI.

The spin-dependent PC  $I_{s,pc}$  is measured by a lock-in amplifier in current detection mode with the laser pump pulses modulated between  $\sigma^+$  and  $\sigma^-$  by a photo-elastic modulator at 42 kHz. Furthermore, we reduce the laser repetition time  $T_{rep}$  to 12.5 ns. It is not a priori obvious that  $I_{s,pc}$  should depend on  $\mathbf{M}_{Fe}$ , since  $\mathbf{S}_{opt}$  is perpendicular to  $\mathbf{M}_{Fe}$  and hence  $\mathbf{S}_{pc}$ . The dynamics of the two spin populations, however, are very different.  $\mathbf{S}_{opt}$  is induced by the optical pulse (width  $\approx 3$  ps), and it will therefore precess about  $B_z$  with a precisely defined phase for time scales up to  $T_2^*$ , which is greater than 50 nanoseconds at low temperatures. The interfacial spin polarization  $\mathbf{S}_{PC}$ , however, is generated over the course of the entire PC

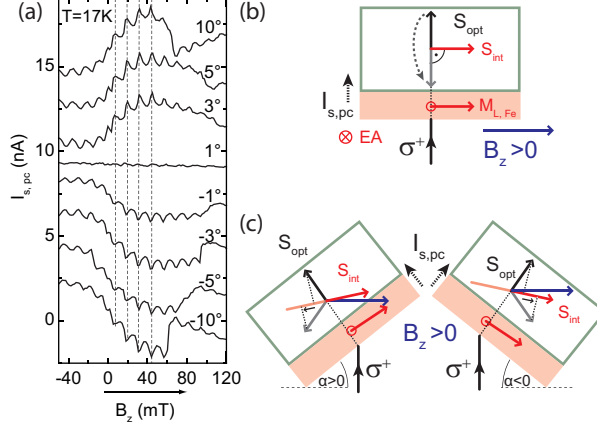


Figure 4: (color online) (a) Spin PC vs  $B_z$  for different angles  $\alpha$  of the magnetic field relative to the Fe/GaAs interface at 17 K. (b) Illustration of sample along  $x$ -direction under normal incidence ( $\alpha = 0^\circ$ ) and (c) for  $\alpha > 0^\circ$  and  $\alpha < 0^\circ$ . The spin polarized PC pulse leads to an interfacial spin accumulation  $\mathbf{S}_{int}$ , which acts as a spin detector for  $\mathbf{S}_{opt}$ . Spin precession of  $\mathbf{S}_{opt}$  about  $B_z$  is observed because of its sensitivity to  $\mathbf{S}_{int}$ . Note that the sign of the precessing component reverses sign upon reversal of  $\alpha$ .

pulse (several nanoseconds).

To probe how these distinct spin populations influence the total PC,  $B_z$  is applied at an angle  $\alpha$  relative to the plane of the Fe/GaAs interface. Fig. 3(f) shows magnetic field loops of  $I_{s,pc}$  with  $\alpha = 6^\circ$  and the EA of the sample almost perpendicular to  $B_z$ . We observe a clear spin-dependence of the PC signal at all  $T$  with abrupt jumps at the coercive fields of the Fe layer, which occur due to a slight misalignment of the EA (approximately  $4^\circ$ ). At low  $T$ , peaks in  $I_{s,pc}$  are observed at regularly spaced intervals of 12.87 mT. These are due to resonant spin amplification [1] of  $\mathbf{S}_{opt}$  when the Larmor period is equal the repetition rate of the optical pulses. In contrast to RSA peaks in TRESI (see Fig. 3(c)), these peaks survive up to larger  $T$  consistent with  $T_2^*$  in the GaAs bulk[1].

At first glance, RSA oscillations in Fig. 3(f) might be attributed to the orientation of the precessing spin polarization  $\mathbf{S}_{opt}$  relative to  $\mathbf{S}_{pc}$ . The relationship, however, is more subtle, as can be seen in Fig. 4(a). Remarkably, when  $\alpha = 0$  there is almost no spin-dependent PC, although the precessing  $\mathbf{S}_{opt}$  does have a significant non-zero projection onto  $\mathbf{S}_{pc}$ , which is rotating from the easy toward hard axis as  $B_z$  increases. A spin-dependent PC appears only when the sample is rotated slightly about the EA, as shown for several angles in Fig. 4(a).

The observed field and angle dependence indicates that  $I_{s,pc}$  is nearly proportional to the *longitudinal* (non-precessing) component of  $\mathbf{S}_{opt}$ , which is oriented along  $B_z$ . This can only be due to the fact that over the course of the bulk  $T_2^*$ -time (the effective duration of the experiment), the time evolution of  $\mathbf{S}_{pc}$  results in an interfacial spin accumulation  $\mathbf{S}_{int}$  that is nearly parallel to  $B_z$ , and not to  $\mathbf{M}_{Fe}$ . The spin current that leads to the observed  $I_{s,pc}$  is driven by the gradient between the spin accumulation in the bulk  $S_{opt}$  and the interfacial spin accumulation  $\mathbf{S}_{int}$ .

An important question is why the direction of  $\mathbf{S}_{int}$  differs from  $\mathbf{S}_{pc}$ . The primary reason is dynamic nuclear polarization (DNP), which leads to rapid precessional dephasing of the transverse component of  $\mathbf{S}_{pc}$  in a hyperfine field that in steady-state points along  $B_z$ . Although this mechanism is well-known[26], a remarkable aspect of the data shown in Fig. 4(a) is that the bulk spins, as indicated by periodic peaks in  $B_z$ , continue to precess at the bare Larmor frequency. This is due to the fact that DNP occurs only in the interfacial region and not in the bulk, which can be polarized only by nuclear spin diffusion, which occurs only very slowly[27, 28]. A second puzzling aspect of the data is that a precessing component of  $\mathbf{S}_{opt}$  is still observable at lower  $T$ , implying that  $\mathbf{S}_{int}$  is not exactly parallel to  $B_z$  for  $\alpha \neq 0$  (see Figs. 4(b) and (c)). There are two possible explanations for this behavior. First, due to the presence of the Knight field of the spin-polarized electrons[28], the hyperfine field, which dominates the spin dynamics in the interfacial region, is not exactly parallel to  $B_z$ . Second, the fact that the effective duration of the experiment is several ns means that  $\mathbf{S}_{int}$  never reaches its steady state orientation along  $B_z$ . A full understanding will require explicit modeling of the spin dynamics on the ns time-scale, which is not in the steady-state in contrast to ordinary spin transport experiments.

In conclusion, we have shown that electrical current pulses can trigger spin packets that are injected across an Fe/GaAs Schottky barrier with a well-defined phase. Charging and discharging of the Schottky barrier yields a temporal broadening of the spin packets resulting in a partial dephasing during spin precession. We also have shown that precession of spin packets generated by optical pulses can be probed electrically due to the spin sensitivity of the resulting photocurrent. These results thus demonstrate that electrical injection and detection of electron spin packets in ferromagnet/semiconductor spin transport devices are feasible at microwave frequencies.

Supported by HGF and by DFG through SPP 1285. Work at Minnesota was supported

by the Office of Naval Research, in part by the NSF NNIN and MRSEC programs (DMR 0819885) and NSF DMR 0804244.

---

\* bernd.beschoten@physik.rwth-aachen.de

- [1] J. M. Kikkawa and D. D. Awschalom, Phys. Rev. Lett. **80**, 4313 (1998).
- [2] J. M. Kikkawa and D. D. Awschalom, Nature **397**, 139 (1999).
- [3] Y. K. Kato *et al.*, Nature **427**, 50 (2003).
- [4] A. Greilich *et al.*, Science **313**, 341 (2006).
- [5] A. V. Kimel *et al.*, Phys. Rev. B **63**, 235201 (2001).
- [6] L. Meier *et al.*, Nature Phys. **3**, 650 (2007).
- [7] K. Schmalbuch *et al.*, Phys. Rev. Lett. **105**, 246603 (2010).
- [8] Y. Ohno *et al.*, Nature **402**, 790 (1999).
- [9] H. J. Zhu *et al.*, Phys. Rev. Lett **87**, 016601 (2001).
- [10] A. T. Hanbicki *et al.*, Appl. Phys. Lett. **80**, 1240 (2002).
- [11] X. Jiang *et al.*, Phys. Rev. Lett. **94**, 056601 (2005).
- [12] C. Adelmann *et al.*, Phys. Rev. B **71**, 121301R (2005).
- [13] P. Kotissek *et al.*, Nature Phys. **3**, 872 (2007).
- [14] M. Ciorga *et al.*, Phys. Rev. B **79**, 165321 (2009).
- [15] S. A. Crooker *et al.*, Science **309**, 2191 (2005).
- [16] B. H. Ian Appelbaum and D. J. Monsma, Nature **447**, 295 (2007).
- [17] B. Huang *et al.* Phys. Rev. Lett. **99**, 177209 (2007).
- [18] B. H. Jing Li and I. Appelbaum, Appl. Phys. Lett **92**, 142507 (2008).
- [19] X. Lou *et al.*, Nature Phys. **3**, 197 (2007).
- [20] Y. K. Kato *et al.*, Appl. Phys. Lett. **87**, 022503 (2005).
- [21] R. I. Dzhioev *et al.*, Phys. Rev. B **66**, 245204 (2002).
- [22] See Supplemental Material for detailed descriptions.
- [23] R.K. Kawakami *et al.*, Science **294**, 5540 (2001).
- [24] R.J. Epstein *et al.*, Phys. Rev. B **65**, 121202 (2002).
- [25] C. Ciuti *et al.*, Phys. Rev. Lett. **89**, 156601 (2002).
- [26] D. Paget *et al.*, Phys. Rev. B **15**, 5780 (1977).

- [27] J. Stephens *et al.*, Phys. Rev. Lett. **93**, 097602 (2004).
- [28] M.K. Chan *et al.*, Phys. Rev. B **80**, 161206R (2009).